Journal of Asian Earth Sciences 74 (2013) 155–166

Contents lists available at SciVerse ScienceDirect

Journal of Asian Earth Sciences

journal homepage: www.elsevier.com/locate/jseaes

Geochemical studies on Permian manganese deposits in Guichi, eastern China: Implications for their origin and formative environments

Jiancheng Xie [a,b,*], Weidong Sun [a,*], Jianguo Du [c], Wei Xu [c], Libing Wu [c], Xiaoyong Yang [d], Taofa Zhou [b]

[a] CAS Key Laboratory of Mineralogy and Metallogeny, Guangzhou Institute of Geochemistry, The Chinese Academy of Sciences, Guangzhou 510640, China
[b] School of Resource and Environmental Sciences, Hefei University of Technology, Hefei 230009, China
[c] Anhui Academy of Geological Survey, Hefei 230001, China
[d] CAS Key Laboratory of Crust-Mantle Materials and Environments, School of Earth and Space Sciences, University of Science and Technology of China, Hefei 230026, China

ARTICLE INFO

Article history:
Received 19 October 2012
Received in revised form 23 March 2013
Accepted 2 April 2013
Available online 11 April 2013

Keywords:
Permian manganese deposit
Sedimentary environment
Hydrothermal
Source of manganese
Guichi region

ABSTRACT

Permian manganese ore deposits are widely distributed in southwestern and eastern China. Guichi Permian manganese district in southern Anhui Province, central eastern China, is currently the most important manganese metal producers in eastern China. Manganese ores (MnO = 18.2–45.4 wt.%) in Guichi region occur in calcareous, argillaceous and siliceous Mn-bearing sequence of the Permian Gufeng Formation. In contrast to Mn-bearing rocks, the ores have higher Mn, Fe, P, Sr (more than 1500 ppm) and Ni contents (>480 ppm), higher Mn/Fe (>5) and La_n/Ce_n (>2) values, and lower Co/Ni (<0.05) ratios. The Guichi manganese deposits also have low Co/Ni (<1) and Co/Zn ratios, low in total REE contents (mostly < 100 ppm) with negative Eu (0.46–0.75) and Ce (0.42–0.76) anomalies. The mineralogy and geochemistry of manganese deposits in the Guichi region strongly indicate hydrothermal activities, which is supported by high paleotemperatures (49–71 °C) of Permian Mn-carbonate ore and Mn-bearing carbonate. The low $Ce_{anom.}$ values (<−0.1) and high strontium contents indicate that the Guichi manganese deposits were formed in high-salinity and oxidative marine sedimentary environment. The Al_2O_3/TiO_2 (9.23–48.2) and Y/Ho (25.9–44.4) ratios, REE patterns, $\delta^{13}C_{V\text{-}PDB}$ (−10.2‰ to 5.00‰) and $\delta^{18}O_{SMOW}$ (20.7–28.0‰) characteristics of Permian manganese deposits reveal a mixed Mn source of volcanic, terrigenous and organic matter.

1. Introduction

Manganese ore deposits are widely distributed in China, which is ranked fifth in the world in terms of total Mn reserves. The sedimentary Mn deposits comprise ~70% of the total Mn reserves of China (Fan and Yang, 1999), and are primarily hosted by mud rock, black shale, carbonate rock, and chert–mudstone–limestone (Fan and Yang, 1999; Fan et al., 1999), and formed during the Proterozoic, Cambrian, Ordovician, Devonian, Carboniferous, Permian, Triassic, Jurassic, Cretaceous and Quaternary (Fig. 1) (Fan and Yang, 1999; Fan et al., 1999; Hein et al., 1999; Liu and Xue, 1999; Tang and Liu, 1999; Xie et al., 2006; Yeh et al., 1999; Zeng and Liu, 1999). Most of the Mn reserves of China are distributed in the Neoproterozoic, Devonian and Permian periods. In contrast, Proterozoic, Devonian, Cretaceous and Oligocene Mn deposits are widely found elsewhere in the world (Fig. 1) (Brusnitsyn and Zhukov, 2012; Fitzgerald and Gillis, 2006; Jach and Dudek, 2005; Munteanu et al., 2004; Nyame, 2008; Nyame et al., 2002; Polgári et al., 2012, 2005; Roy, 2006; Salas et al., 2008; Sethumadhav et al., 2010).

Permian manganese deposits, which typically show a Si–Ca–Mn element association (Fig. 1), are mainly distributed to the south of the Yangtze River in China (Fig. 2). The main deposits are the Gexue medium-sized manganese deposit (2–20 million tonnes reserve and Mn grade >18% according to China standard) in Yunnan Province; the Shuicheng (medium), Nayong (medium) and Zunyi (large, >20 million tonnes reserve) manganese deposits in Guizhou Province; the Bayi (large), Pinglu, Lipu and Fenghuang (medium) manganese deposits in Guangxi Province; the Dongxiang (large, Qiyang-Lingling), Dongshanxia (medium) manganese deposits in Hunan Province; the Daye, Jiayu and Hongan (medium) manganese deposits in Hubei Province; and the Guichi manganese deposit (medium) in Anhui Province (Fig. 2).

The Guichi manganese district is situated in southern Anhui Province, which is currently the most important manganese metal producers in eastern China (Xie et al., 2006). Mn-ore reserve and resource of Guichi manganese district are about 2.3 million tonnes (>18% Mn) and 5.0 million tonnes, respectively (Table 1). In contrast to Mn ore deposits in northeast and southwest of China, which have been studied in detail (Fan and Yang, 1999; Fan et al., 1999; Hein et al., 1999; Liu and Xue, 1999; Liu et al., 2008; Tang and Liu, 1999; Yang et al., 2009; Zeng and Liu, 1999), the Mn deposits in eastern China has rarely been studied (Xie et al., 2006).

* Corresponding authors. Tel.: +86 0551 2901524.
E-mail addresses: xiejiancheng08@163.com (J. Xie), weidongsun@gig.ac.cn (W. Sun).

1367-9120/$ - see front matter © 2013 Elsevier Ltd. All rights reserved.
http://dx.doi.org/10.1016/j.jseaes.2013.04.002

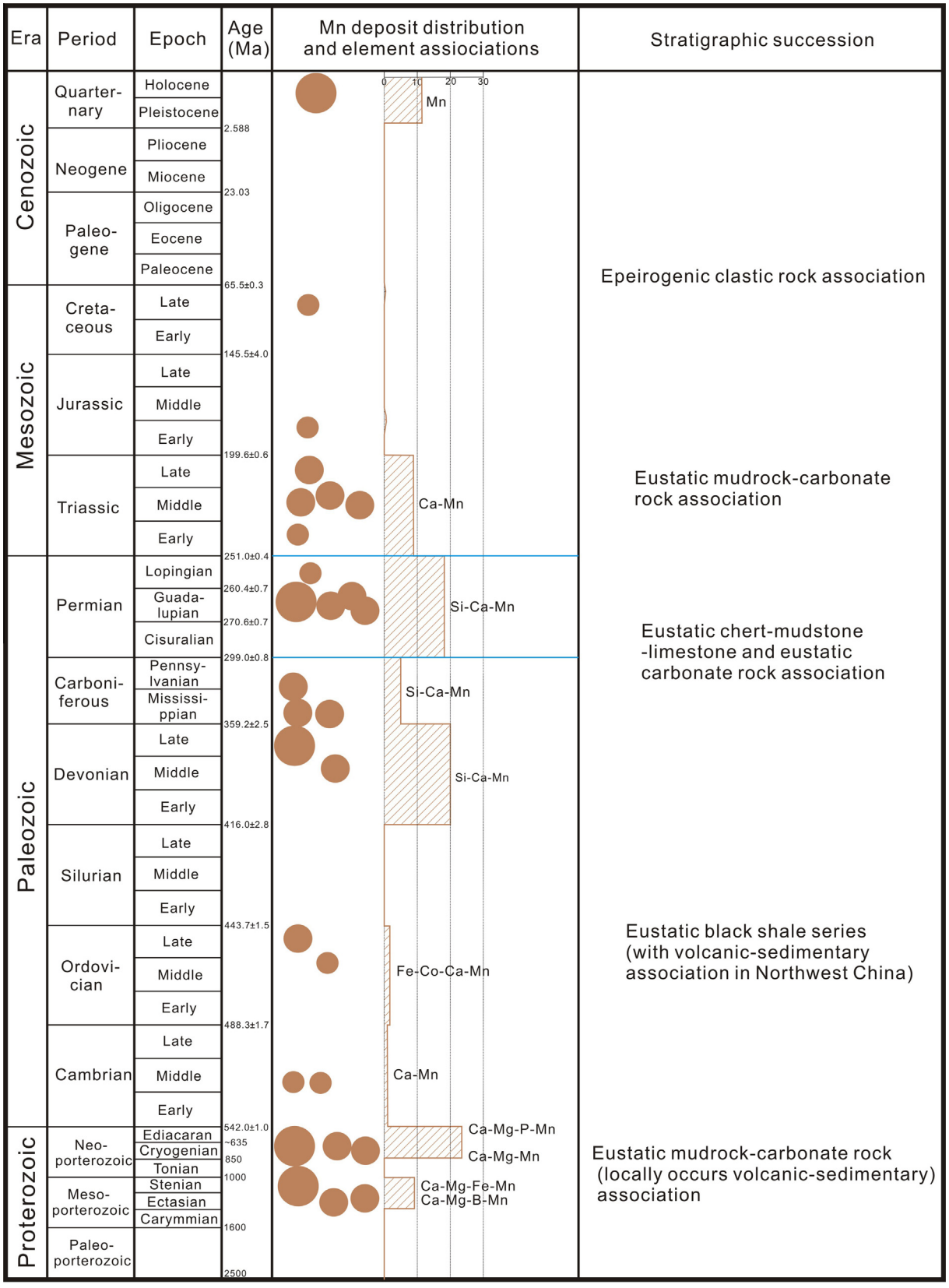

Fig. 1. Temporal–stratigraphic distribution and element associations of manganese deposits in China (modified from Fan and Yang, 1999). Brown solid circles of different sizes stand for large (>20 million tonnes reserve), medium (2–20 million tonnes reserve) and small (<2 million tonnes reserve) of manganese ore deposits, respectively. (For interpretation of the references to color in this figure legend, the reader is referred to the web version of this article.)

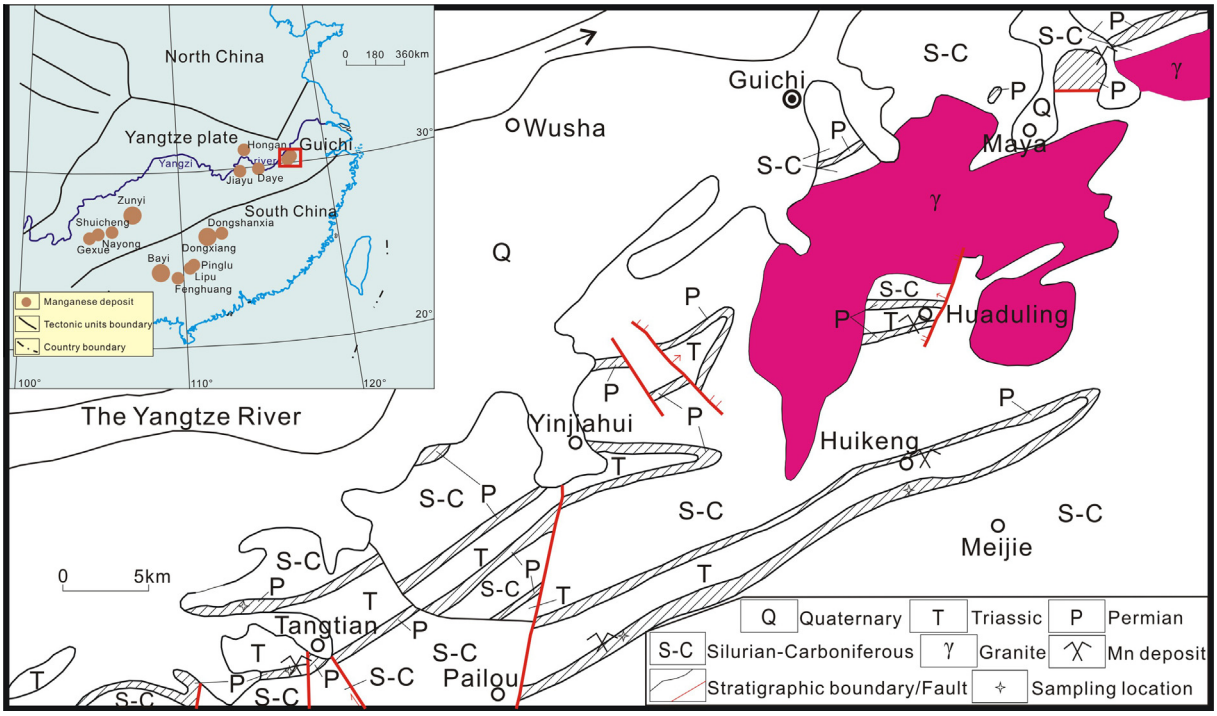

Fig. 2. Geological map of sedimentary manganese deposits of the Guichi region (modified from Xie et al., 2006).

This contribution aims to provide firmer constraints on the formation of the Permian manganese deposits in the Guichi region and in southern China in general, using petrographic, stratigraphic and geochemical data.

2. Geological characteristics of Guichi manganese deposits

2.1. Geological setting

The Guichi Mn ore district includes Tangtian, Pailou, Huikeng, Huaduling and Maya sedimentary manganese deposits (Fig. 2 and Table 1) (Xie et al., 2006). These deposits occur in the Permian Gufeng Formation (Figs. 2 and 3) and are primarily distributed in the two limbs of the Guichi's synclinorium (Fig. 2). They are composed of silicalite, siliceous shale, argillaceous (calcareous) shale, Mn-bearing limestone, Mn-bearing shale, wad, and a Mn-ore layer (Fig. 3). The thickness of the Gufeng Formation varies dramatically, from 50 to 212 m at Tangtian deposit, to >100 m at Pailou deposit and 79.8–104 m at Huikeng deposit (Figs. 2 and 3).

Tectonically, the Guichi manganese ore district is situated along the northern margin of the Yangtze craton in eastern China (Fig. 2). Cambrian to middle Triassic sedimentations developed on stable Precambrian basement, forming a thick sedimentary sequence (Chang et al., 1991; Xie et al., 2006) (Fig. 2). Regional structures include "S" type fold of the Guichi synclinorium and NE and NW trending faults that controlled the distribution of these manganese deposits. This region has long been interpreted as an intraplate deformation with abundant magmatism during the Yanshanian

Table 1
Characterists of manganese deposits from Guichi region.

Name of deposit	Length of Mn-bearing sequence (km)	Shape of ore body	Length of ore body (m)	Mean thickness of ore body (m)	Ore type	Main composition (wt.%)				Mn-ore reserves (10^6 ton)	Mn-ore resources (10^6 ton)
						MnO	TFe	P_2O_5	SiO_2		
Tangtian	20.5	Layers or like-layers	12,400	1.56	Native manganese carbonate ore and manganese oxide ore	19.5–41.3	3.03–6.57	0.03–0.27	16.7–42.4	1.05	1.39
Pailou	24.0	Layers or like-layers	14,000	1.91	Native manganese carbonate ore and manganese oxide ore	18.2–38.0	1.97–3.07	0.12–0.22	14.6–20.3	0.48	1.63
Huikeng	16.0	Layers or like-layers	10,500	1.00	Native manganese carbonate ore and manganese oxide ore	21.9–45.4	3.74–10.4	0.13–0.70	11.2–28.1	0.39	1.09
Maya	5.50	Layers or like-layers	About 2000	0.93	Manganese oxide ore	40.2				0.18	0.37
Huaduling	4.00	Layers or like-layers	About 2300	0.82	Manganese oxide ore	27.5		0.05		0.15	0.54

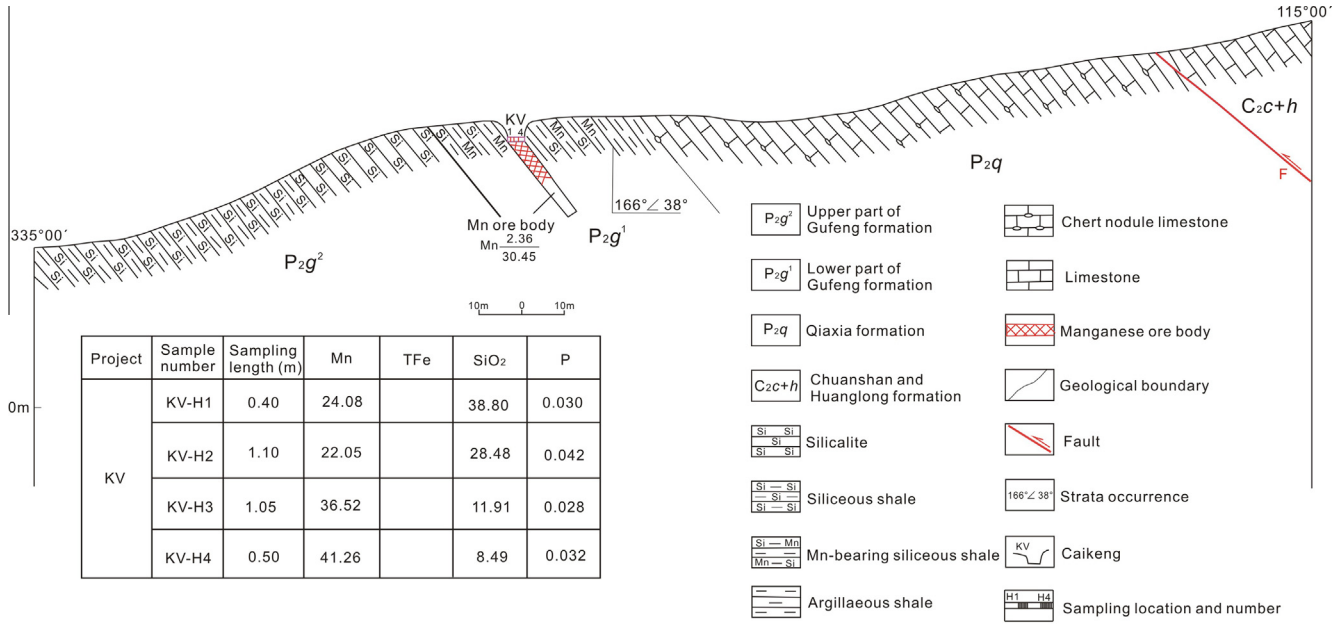

Project	Sample number	Sampling length (m)	Mn	TFe	SiO_2	P
KV	KV-H1	0.40	24.08		38.80	0.030
	KV-H2	1.10	22.05		28.48	0.042
	KV-H3	1.05	36.52		11.91	0.028
	KV-H4	0.50	41.26		8.49	0.032

Fig. 3. Geological section of manganese deposits of the Guichi region.

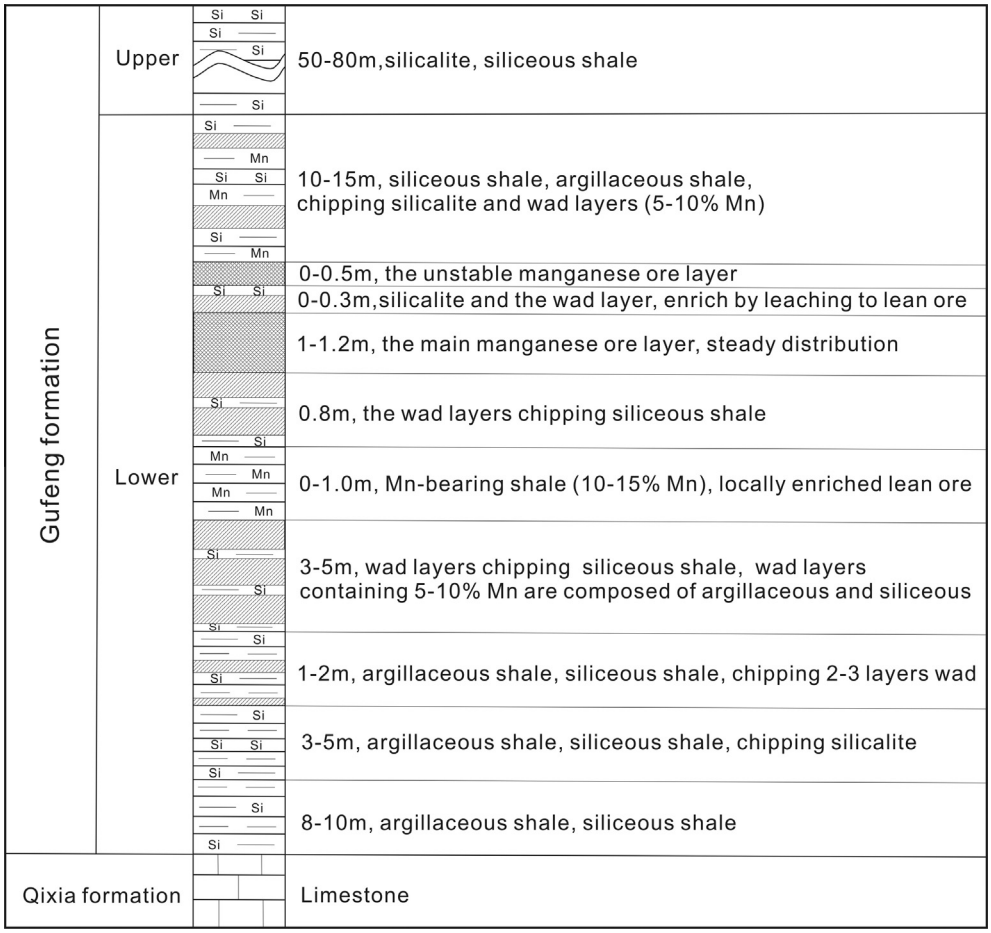

Fig. 4. Stratigraphic section for the Mn-bearing sequence of the Tangtian manganese deposit.

Table 2
Major element compositions (wt.%) of manganese deposits from Guichi area.

Sample	Rock (ore) type	SiO_2	TiO_2	Al_2O_3	Fe_2O_3T	MnO	MgO	CaO	Na_2O	K_2O	P_2O_5	SO_3	LOI	Total	Al_2O_3/TiO_2	Mn/Fe
GH1	Mn-bearing limestone	32.9	0.18	4.20	3.07	2.80	1.45	26.8	0.05	0.86	0.38	3.48	26.6	102.7	23.3	0.98
GH2	Mn-bearing limestone	37.7	0.14	3.03	3.64	1.76	1.30	25.6	0.05	0.49	0.30	5.03	25.2	104.1	21.6	0.52
GH3	Mn-bearing limestone	30.3	0.08	1.35	1.07	4.18	2.01	30.9	0.04	0.24	0.49	1.55	28.5	100.7	17.5	4.20
GH4	Mn-bearing limestone	39.9	0.04	1.08	1.18	3.90	3.14	24.8	0.04	0.16	0.34	1.62	24.8	101.1	27.7	3.56
GH5	Silicalite	53.6	0.13	3.80	4.77	2.88	1.08	12.6	0.05	0.51	0.51	8.31	19.5	107.7	29.2	0.65
GH6	Silicalite	86.2	0.11	2.55	0.57	0.03	0.17	0.23	0.04	0.36	0.03	1.08	8.97	100.4	23.2	0.06
GP1	Limestone	14.8	0.03	1.09	0.55	0.10	0.54	44.7	0.03	0.14	0.03	1.02	37.2	100.2	34.1	0.20
GP2	Silicalite	84.7	0.01	0.28	0.29	0.04	0.15	7.08	0.03	0.05	0.02	0.27	6.84	99.7	36.8	0.15
GP3	Manganese ore	6.52	0.01	0.46	0.56	20.7	2.92	33.3	0.03	0.08	0.15	1.04	34.2	99.9	41.8	39.7
GP4	Mn-bearing limestone	24.5	0.04	1.83	1.53	8.87	2.51	30.1	0.03	0.26	0.77	0.15	29.0	99.6	48.2	6.24
GP5	Silicalite	95.0	0.03	0.90	0.49	0.22	0.09	0.49	0.04	0.11	0.09	0.22	1.88	99.6	28.1	0.48
GP6	Mn-bearing limestone	5.96	0.02	0.58	0.48	4.62	1.22	46.8	0.06	0.11	0.29	0.62	39.0	99.7	38.7	10.4
GT1	Mn-bearing siliceousshale	74.7	0.19	5.18	3.87	9.96	0.31	0.31	0.05	0.55	0.12		4.36	99.6	27.3	2.77
GT2	Manganese ore	39.4	0.15	4.29	3.52	40.0	0.25	0.48	0.12	0.65	0.33		7.95	97.1	28.6	12.2
GT3	Mn-bearing siliceous shale	63.4	0.34	7.02	8.66	11.3	0.8	0.85	0.24	1.17	0.19		5.90	99.9	20.6	1.41
GT4	Mn-bearing shale	81.8	0.17	4.74	3.52	4.62	0.36	0.30	0.05	0.45	0.14		3.34	99.5	27.9	1.41
GT5	Manganese ore	57.9	0.16	3.86	3.51	24.6	0.42	0.55	0.12	0.58	0.25		6.49	98.4	24.1	7.53
GT6	Manganese ore	43.6	0.24	6.69	5.34	30.5	0.18	0.13	0.04	0.19	0.30		11.2	98.4	27.9	6.15
GT7	Mn-bearing siliceous shale	77.3	0.19	4.89	3.32	7.60	0.45	0.15	0.94	0.02	0.07	0.03	4.41	99.4	25.7	2.46
GT8	Siliceous shale	74.2	0.34	8.34	9.12	0.77	0.75	0.05	1.60	0.04	0.23	0.03	3.92	99.4	24.5	0.09
GT9	Manganese ore	45.9	0.24	11.4	4.82	22.4	0.51	0.37	1.09	0.05	0.13	0.03	10.7	97.6	47.4	5.00

period (Jurassic/Cretaceous) (Fig. 2), which is now attributed to a ridge subduction (Li et al., 2012a, 2011; Ling et al., 2009, 2011; Sun et al., 2010).

2.2. The Mn-bearing sequence and manganese ore body

The Mn-bearing sequence in the Guichi region is composed of Mn-bearing calcareous, argillaceous, and siliceous marine sedimentary assemblages occurrence in the lower part of the Gufeng Formation with a length of 4–24 km (Figs. 2–4 and Table 1). The manganese ore bodies are rich and thick as the Mn-bearing sequence becomes increasingly calcareous and argillaceous. In comparison, the manganese ore bodies become thinner or even disappeared when the Mn-bearing sequence becomes more siliceous. These are useful signs for Mn ore prospection in this region.

The length of individual manganese ore bodies in the Guichi region range from ~2 km to 12.4 km (Figs. 3 and 4; Table 1). The ore layers are generally conformable with the geologic strata (Fig. 3). The Mn ore typically occurs as a single layer, with sharp upper and bottom contacts with adjacent barren interbed (Figs. 3 and 4). Overlyings of manganese ore bodies are Mn-bearing shale, siliceous shale, and argillaceous shale containing wad layers. Underlyings of manganese ores are shale, siliceous shale and wad, containing the abundant fossils (Figs. 3 and 4). The hanging and foot walls of ore bodies are enriched in calcareous and argillaceous materials. Ore bodies in extension usually have good continuity, with thicknesses of 0.82–1.91 m (Xie et al., 2006) (Figs. 3 and 4; Table 1), and were influenced by oxidation secondary enrichments. Manganese ore layer has obvious vertical zoning characteristics. Rich oxide manganese ore with layered characteristics is formed by oxidation of manganese carbonate ore in the upper part. The lower part is primary depositional manganese carbonate ore.

2.3. Ore type and component

Manganese deposits in the Guichi region are primarily divided into primary manganese carbonate ore and manganese oxide ore. Manganese oxide ore is primarily composed of pyrolusite and psilomelane, with manganite. The gangue minerals are mainly quartz, limonite, and sericite. Manganite ores have massive and layered structures, generally expressed as inter-bedded manganite layers with argillaceous and calcareous shale. Pyrolusite ores with massive or bedded structures are composed of needle and radial aggregates of pyrolusite, resembling the texture of the primary sedimentary manganite ores. Psilomelane ores have lamination, reniform, mammillary, needle, zonal structures and cryptocrystal texture. Primary manganese carbonate ores have massive, earthy, spheroidal, or conglomeratic structures and granular textures. Primary manganese carbonate ore is composed of rhodochrosite and Mn calcite.

3. Samples and analytic methods

Thirty-six samples taken from outcrops at Tangtian, Pailou and Huikeng manganese deposits across ore bodies were studied in this contribution (Fig. 2). Major and trace element (including REEs) compositions of 21 samples were analyzed. Among them, five samples were ores, 11 samples were from the Mn-bearing sequence, and five samples were from non-ore host rocks.

About 500 g chips for each sample were carefully selected, washed with distilled water at room temperature, and then dried at 105 °C. The chip samples were ground to less than 200 meshes using an agate mill. Major and trace elements were analyzed in the Anhui Geological Laboratory of the Anhui Geological Bureau. Major element oxides were determined using X-ray fluorescence spectroscopy, minor elements using inductively coupled plasma-atomic emission spectrometry (ICP-AES), and rare earth elements (REEs) using ICP-mass spectrometry (MS). Carbon and oxygen isotopes of eight carbonate samples were measured using CO_2 evolved by phosphorolysis in 100% H_3PO_4 using a Finnigan MAT-251 mass spectrometer at the Institute of Mineral Resources, Chinese Academy of Geological Sciences. The precision is ±0.2‰ for $\delta^{13}C$ and $\delta^{18}O$. The analytical results are presented in Tables 2–4, respectively.

4. Results

4.1. Major elements

Major element compositions are listed in Table 2. Loss on ignition (LOI) ranges from 1.88 wt.% to 39.0 wt.% (with an average of 16.2 wt.%). High LOI contents are consistent with a high percentage of calcite and clay minerals. The MnO contents of Mn-ore, Mn-bearing sequence and wallrock samples range from 18.2 wt.% to 45.4 wt.%, 1.76 wt.% to 11.3 wt.%, and 0.03 wt.% to 0.77 wt.%,

Table 3
Trace element compositions (ppm) of manganese deposits from Guichi region.

Sample	Ba	Rb	Sr	Y	Nb	Pb	Zn	Cu	Ni	V	Cr	Sc	Co	Mo	La	Ce	Pr	Nd	Sm	Eu	Gd	Tb	Dy	Ho	Er	Tm	Yb	Lu	REE	$Ce^*_{chrodrite}$	Ce^*_{shale}	$(La/Yb)_N$	Ceanom.
GH1	53.9	34.6	1350	18.4	7.10	19.0	115	33.5	102	77.3	85.6	4.30	6.60	7.08	18.3	28.5	4.24	15.1	2.48	0.55	3.39	0.46	2.51	0.57	1.49	0.25	1.38	0.22	79.4	0.76	0.75	6.74	−0.12
GH2	41.8	22.0	1634	19.7	5.80	23.1	97.4	31.6	63.3	71.5	82.7	4.30	6.60	9.75	19.9	27.7	4.10	14.0	2.52	0.54	3.06	0.39	2.31	0.49	1.36	0.22	1.25	0.19	78.0	0.71	0.69	7.42	−0.14
GH3	33.5	8.20	1712	22.2	5.40	14.4	102	24.2	74.9	86.3	29.2	2.60	3.40	18.2	19.0	18.5	3.43	11.2	2.52	0.55	3.01	0.38	2.39	0.50	1.44	0.21	1.23	0.18	64.5	0.52	0.50	5.91	−0.28
GH4	22.3	5.30	1203	12.2	2.50	17.8	151	25.5	95.7	79.2	31.9	1.25	2.60	9.28	13.2	10.0	2.03	5.80	1.32	0.30	2.08	0.30	1.53	0.31	0.92	0.15	0.76	0.11	38.8	0.42	0.41	5.30	−0.36
GH5	41.8	27.1	563	40.2	8.90	18.4	248	37.5	223	174	87.6	5.50	13.2	41.1	35.3	36.6	6.28	22.0	5.28	1.06	5.92	0.82	4.97	1.06	2.82	0.40	2.30	0.35	125	0.56	0.54	5.71	−0.26
GH6	67.2	20.0	47.0	6.80	5.10	7.00	9.50	10.5	12.1	486	289	3.00	2.50	20.1	9.40	14.4	2.27	7.90	1.18	0.18	0.85	0.10	0.86	0.19	0.76	0.11	0.78	0.10	39.1	0.74	0.72	9.42	−0.13
GP1	5.00	3.00	1708	9.10	2.80	12.7	41.0	29.1	22.3	143	69.1	1.50	1.40	5.51	14.1	16.5	1.69	8.40	1.30	0.28	2.18	0.30	1.30	0.29	0.93	0.18	0.75	0.10	48.3	0.70	0.67	7.01	−0.20
GP2	15.0	4.30	288	6.10	1.70	8.10	11.4	9.30	8.80	57.4	28.0	1.00	1.40	5.00	5.30	5.30	1.33	4.20	0.69	0.18	1.47	0.15	0.79	0.17	0.50	0.09	0.42	0.07	20.7	0.48	0.47	4.64	−0.30
GP3	28.7	3.00	2204	12.3	2.50	17.0	82.3	20.1	129	104	35.5	1.15	1.00	1.19	13.5	9.40	1.92	6.05	1.26	0.29	2.09	0.31	1.69	0.41	0.96	0.14	1.14	0.12	39.3	0.40	0.38	4.73	−0.40
GP4	37.7	6.90	1950	23.9	3.90	19.3	133	27.5	84.5	104	37.6	1.80	1.00	8.99	18.9	17.8	3.01	10.1	2.39	0.42	3.18	0.50	2.84	0.61	1.74	0.24	1.62	0.24	63.6	0.52	0.50	4.80	−0.28
GP5	52.6	7.90	71.8	8.30	3.00	9.00	35.6	14.2	34.3	71.4	173	1.40	2.90	8.99	5.10	5.30	1.04	4.10	0.95	0.19	1.21	0.12	0.91	0.20	0.56	0.10	0.55	0.08	20.4	0.53	0.52	4.47	−0.29
GP6	29.7	3.00	3360	8.15	1.00	13.5	51.5	31.9	36.8	49.3	40.0	0.95	1.20	1.54	7.50	6.00	1.20	4.65	0.98	0.19	1.60	0.18	0.98	0.25	0.66	0.12	0.53	0.08	24.9	0.44	0.43	4.66	−0.37
GT1	172	40.1	717	23.9	6.50	14.2	473	32.5	437	254	148	6.06	7.50	34.0	29.3	34.9	5.79	21.3	4.51	0.99	4.38	0.65	3.56	0.79	2.17	0.33	1.83	0.32	111	0.62	0.60	6.89	−0.22
GT2	390	38.6	2167	67.7	6.10	12.2	854	49.3	663	973	171	6.78	13.8	34.0	58.4	60.9	12.5	49.8	11.3	2.61	11.7	1.70	9.49	2.05	5.33	0.71	3.89	0.60	231	0.53	0.51	5.52	−0.30
GT3	150	64.3	132	41.7	13.0	28.0	227	44.1	391	588	210	8.16			47.3	60.2	8.45	31.6	6.51	1.37	6.52	0.96	5.15	1.14	2.95	0.44	2.45	0.33	175	0.68	0.66	7.80	−0.18
GT4	153	36.9	454	18.3	5.30	12.2	192	32.3	252	173	97.0	6.80	17.6	4.0	24.6	31.4	4.77	18.5	4.06	0.87	4.95	0.52	2.88	0.62	1.62	0.24	1.45	0.20	96.7	0.67	0.65	6.75	−0.19
GT5	177	39.0	1555	26.2	4.70	8.90	444	30.9	486	432	147	6.39	22.9	14.2	29.4	27.6	5.01	20.9	4.15	1.09	4.68	0.64	3.83	0.83	2.01	0.32	1.76	0.28	103	0.51	0.49	6.15	−0.32
GT6	412	57.9	1962	59.3	9.70	22.9	573	39.5	748	657	157	8.94	15.8	18.0	57.2	50.4	10.3	43.4	8.94	2.24	9.75	1.38	8.11	1.72	4.39	0.64	3.69	0.54	203	0.47	0.46	5.71	−0.35
GT7	392	43.0	1555	26.5	11.8	30.6	222	54.1	188	102	64.4	7.75	14.3	18.3	22.0	48.1	5.49	21.0	4.60	1.06	4.24	0.62	3.40	0.74	2.07	0.31	2.10	0.29	116	1.04	1.02	7.42	0.01
GT8	162	83.8	163	29.4	27.4	36.5	257	43.7	228	318	476	9.95	15.6	67.4	25.2	22.5	3.93	12.8	2.36	0.58	2.66	0.42	2.53	0.70	2.06	0.33	1.98	0.33	78.4	0.50	0.48	6.12	−0.30
GT9	391	61.0	1531	64.8	14.8	32.1	821	42.0	837	270	106	12.7	12.0	28.7	43.7	43.2	11.8	40.0	9.83	2.18	10.2	1.39	6.98	1.46	3.56	0.59	3.44	0.47	179	0.46	0.45	5.36	−0.33

$Ce^* = 2 * Ce_N/(La_N \times Pr_N)$. The shale and chondrite-normalized values after Gromet et al. (1984) and Sun and McDonough (1989).

respectively (Tables 1 and 2; Fig. 3). In contrast to wallrock, Mn-bearing samples are depleted in Ca and Si, but relatively enriched in Mn, Fe and P. Fe_2O_{3T} and P_2O_5 contents decrease with increasing MnO in the Mn-bearing samples. MnO/TiO_2 ratios are consistently lower (<10) in wallrocks, compared to the Mn-bearing sequence (12.6–308) and ore (up to 1877).

The bulk rock analyses are characterized by low Al_2O_3 (0.28–11.4 wt.%; with an average of 3.69 wt.%) and total alkali ($K_2O + Na_2O$) contents (0.07–1.64 wt.%) and high Fe_2O_{3T} contents (0.29–9.12 wt.%; with an average of 3.04 wt.%) (Table 2). Samples from the Guichi manganese deposits have high Al_2O_3/TiO_2 (17.5–48.2) (Fig. 5A and Table 2), which is very similar to those (11–43) of the rhyolites and tuffs in the upper sequence of the lava succession at Binchuan in western Yunnan Province of China (Xu et al., 2010). The four highest Al_2O_3/TiO_2 ratios (38.7–48.2) are noted for samples GP3, GP4, GP6 and GT9, with values typical of felsic volcanic rocks (Hayashi et al., 1997).

4.2. Trace elements

The trace element contents vary significantly in Guichi manganese deposits (Table 3). Ni contents of Mn-ore, Mn-bearing sequence and wallrock samples are >480 ppm, 50–400 ppm and <50 ppm, respectively. Co/Ni ratios of all samples are less than 1 (Fig. 5B and Table 3). The Sr and Ba concentrations in the Guichi manganese deposits are in the range of 332–3360 ppm and 22.3–412 ppm, respectively and are distinctly enriched in Mn ores and the Mn-bearing sequence. Sr/Ba ratios of all samples vary between 0.70 and 113, and are lower in wallrocks compared to Mn ores and the Mn-bearing sequence (Fig. 5B).

The studied samples have total REE of 20.4–231 ppm with coherent REE patterns characterized by relative enrichments of LREE and nearly flat HREE ($(La/Yb)_N = 6.65–13.9$), moderately negative Eu (0.46–0.75) and Ce (0.42–0.76; with the exception of one sample) (Table 3) anomalies (Fig. 6A). These are distinctly different from those of hydrogenous deposits (Oksuz, 2011 and references therein), but are similar to those of hydrothermal origins (Oksuz, 2011 and references therein) (Fig. 6A). In a SCNA-normalized trace elements spider diagram, all samples have similar patterns with distinct Sr, Ni enrichments, and Rb depletion, indicating that those deposits formed in similar environments and/or with similar sources (Fig. 6B).

In a La_n/Ce_n vs. $Al_2O_3/(Al_2O_3 + Fe_2O_3)$ diagram, the samples mainly plot in the pelagic field (Fig. 7) (Murray, 1994). Two samples (Mn-ore and Mn-bearing rock) plot between the pelagic and ridge fields (Fig. 7).

4.3. C and O isotopes

Oxygen and carbon isotopic data of Mn carbonate ore and Mn-bearing carbonate are listed in Table 4. With the exception of one sample, the $\delta^{13}C_{V\text{-}PDB}$ values (−4.1‰ to 5‰) are plot in the field of marine carbonates, indicating that carbon was primarily derived from Permian seawater (Fig. 8) (Hein and Kosk, 1987; Irwin et al., 1977; Okita et al., 1988; Yeh, 1997; Zeng and Liu, 1999). One negative $\delta^{13}C_{V\text{-}PDB}$ value (−4.1‰ of GP6) of Guichi region implies contribution of carbon from marine organic matter ($\delta^{13}C_{V\text{-}PDB} = -6‰ \sim -19‰$) (Zheng and Chen, 2000) likely oxided by sulfate-reducing bacteria during early diagenesis as proposed by Lafaye and Weber (2003). The $\delta^{18}O_{SMOW}$ values of all samples range from 20.7‰ to 27.4‰, with an average of 23.4‰ (Table 4 and Fig. 8). The homogeneous oxygen isotopic values for the Mn-bearing limestone and Mn carbonate ores seem to indicate a similar marine source and comparable temperatures during precipitation and diagenesis of the different Mn-bearing limestone (Pfeifer et al., 1988).

Table 4
C and O isotopic compositions for Permian manganese deposits.

Location	Sample	Rock (ore) type	$\delta^{13}C_{V\text{-}PDB}$‰	$\delta^{18}O_{V\text{-}PDB}$‰	$\delta^{18}O_{SMOW}$‰	t °C	Data source
Guichi	GP1	Mn-bearing limestone	3.40	−8.60	22.0	62.6	This study
	GP3	Mn carbonate ore	1.00	−3.40	27.4	32.7	
	GP6	Mn-bearing limestone	−4.10	−9.90	20.7	71.2	
	GH1	Mn-bearing limestone	2.80	−8.50	22.1	62.0	
	GH2	Mn-bearing limestone	5.00	−7.90	22.8	58.2	
	GH3	Mn-bearing limestone	2.30	−6.80	23.9	51.5	
	GH4	Mn-bearing limestone	0.60	−7.30	23.4	54.5	
	GT10	Mn-bearing limestone	2.80	−6.30	24.4	48.5	
Zunyi		Mn carbonate ore	−3.96	−6.36	24.4	48.9	Liu et al., 2008
		Mn carbonate ore	−10.2	−6.50	24.2	49.7	
		Mn carbonate ore	−5.29	−5.19	25.6	42.2	Liu et al., 1989
		Mn carbonate ore	−7.77	−5.50	25.2	43.9	
		Mn carbonate ore	−8.09	−4.94	25.8	40.8	
		Mn carbonate ore	−2.97	−4.86	25.9	40.4	
		Mn carbonate ore	−6.16	−2.95	27.9	30.4	
		Siliceous limestone	0.01	−6.58	24.1	50.2	
		Siliceous limestone	0.74	−5.72	25.0	45.2	
		Siliceous limestone	1.97	−6.27	24.4	48.3	
Nayong		Mn-bearing limestone	−4.78	−2.79	28.0	29.6	Liu et al., 2008
		Limestone	3.03	−8.08	22.6	59.3	
		Limestone	1.91	−6.36	24.4	48.9	
Xuanwei		Limestone	−3.88	−9.78	20.8	70.4	

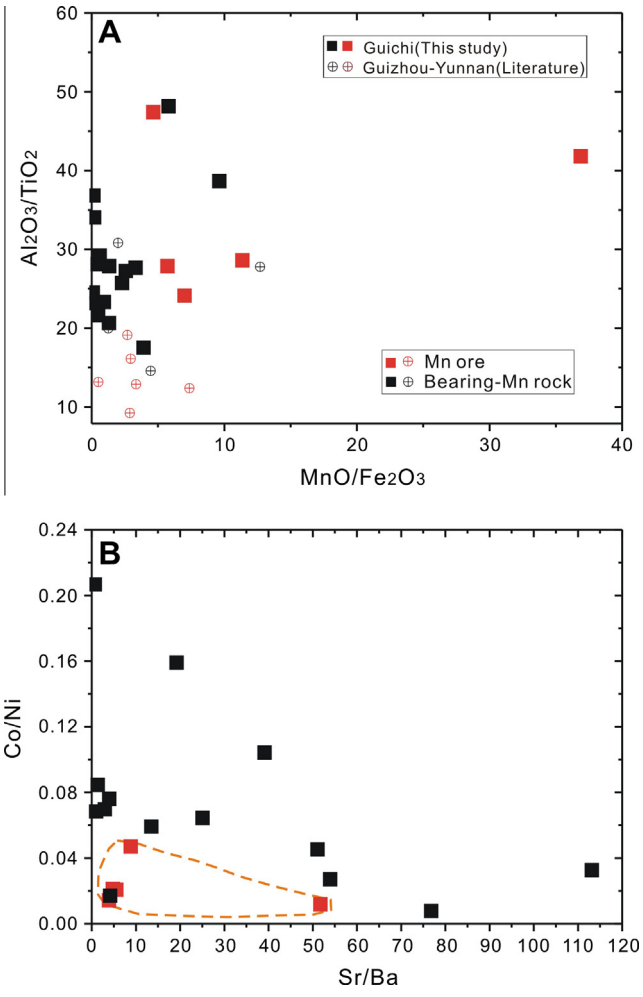

Fig. 5. MnO/Fe_2O_3 vs. Al_2O_3/TiO_2 (A) and Sr/Ba vs. Co/Ni (B) diagrams of Guichi manganese deposits. Data for Guizhou–Yunnan are from Liu et al. (2008).

Oxygen isotope ratios of biogenic calcite may be used to reconstruct palaeotemperature if the calcite was precipitated in isotopic equilibrium with seawater and a diagenetic alteration of the primary isotope ratios can be ruled out. Previous authors proposed that oxygen isotope ratios of belemnite calcite represent equilibrium precipitation and that the ratios may be used to reconstruct palaeotemperature (Fürsich et al., 2005; Price and Sellwood, 1997; Rosales et al., 2004; Wierzbowski, 2002, 2004). Palaeotemperatures were calculated using the equation given by Zheng and Chen (2000) assuming a $\delta^{18}O$ value for Permian seawater of 0‰. The palaeotemperatures of Mn-carbonate samples range from 49 °C to 71 °C with the exception of one sample which gave a value of 33 °C (Table 4).

5. Discussion

5.1. Sources of manganese

Ce/La ratios of samples from Permian manganese ores in China range from 0.60 to 2.19 (average 1.16) (Table 3) (Liu et al., 2008; Yang et al., 2009), suggesting multiple sources. Ce/La ratio is a good indicator of the degree of Ce depletion in sediments (Dubinin and Volkov, 1986). A low Ce/La ratio (~0.12) indicates a large portion of the REE fraction associated with hydrogenous iron- and manganese-hydroxides and adsorbed from sea water. Ce/La ratio increases with increasing carbonaceous biogenic and terrigenous materials and therefore, high Ce/La ratio stands for addition of terrigenic materials, e.g., the ratio is 2.3 in average in the pelagic clays of the Pacific Ocean (Dubinin and Volkov, 1986). The Y/Ho ratios are also indicative of Mn sources (Hein et al., 1999). The Y/Ho ratios of Permian samples collected here vary from 25.9 to 44.4 (mean 36.1) (Table 3) (Liu et al., 2008; Yang et al., 2009), and fall among seawater ratios (range 44–47) (Bau et al., 1996), shales, chondrites, the lithosphere and most volcanic rocks ratios (range 25–28) (McLennan, 1989), and hydrothermal water (Y/Ho = 26–27) (Pack et al., 2007; Sugahara et al., 2010), indicating multiple sources.

The Al_2O_3/TiO_2 ratios of the Guichi manganese deposits range from 17.5 to 48.2 (Table 2), systematically higher than those of

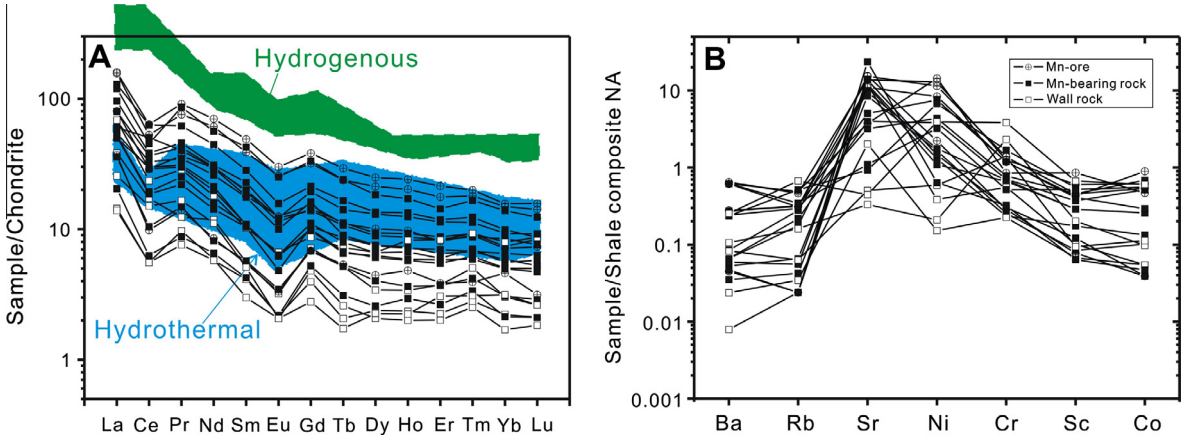

Fig. 6. Rare earth element patterns (A) and spider trace element variation diagrams (B) of Guichi manganese deposits. Data source: Chondrite normalized values (Sun and McDonough, 1989) and SCNA normalized values (Gromet et al., 1984), respectively. The fields of hydrogenous and hydrothermal REE patterns are from Oksuz, 2011 and references therein.

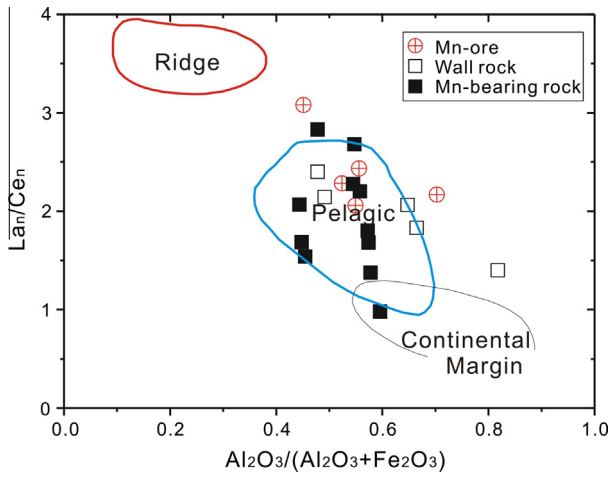

Fig. 7. Plot of La_n/Ce_n vs. $Al_2O_3/(Al_2O_3 + Fe_2O_3)$ for the Guichi manganese deposits. Fields of ridge, pelagic, and continental margin are from Murray (1994). where "*n*" indicates NASC normalized abundance (Gromet et al., 1984).

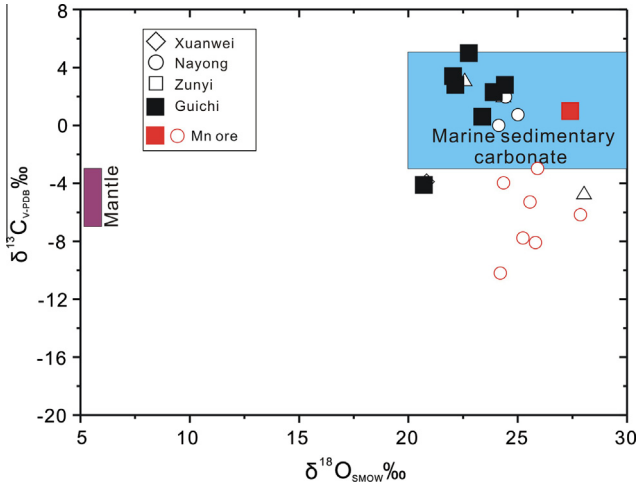

Fig. 8. C–O isotopic components diagram for Permian manganese deposits in China. Some samples of Permian manganese deposits plot in the field of marine sedimentary carbonate, other samples fall outside the field of marine sedimentary carbonate, especially Mn ore samples from Zunyi manganese deposit, indicating two Mn-forming sources. Data source: Mantle (Harmon and Hoefs, 1995; Hoefs, 1997; Mattey et al., 1994); Marine sedimentary carbonate (Hoefs, 1997); Xuanwei, Nayong and Zunyi (Liu et al., 2008; Liu et al., 1989).

the Yunnan–Guizhou manganese deposits (9.23–30.8) (Fig. 5A), which is very similar to that of the felsic volcanic rocks at Binchuan in western Yunnan Province of China (11–43) (Xu et al., 2010). Especially, Al_2O_3/TiO_2 ratios of samples GP3, GP4, GP6 and GT9 from Guichi region are as high as 38–40, which is typical of felsic volcanic rocks (Hayashi et al., 1997). Al_2O_3/TiO_2 ratio is the most useful indicator for the provenance of sedimentary rocks (Hayashi et al., 1997; Taylor and Mclennan, 1985) and acidic tuffs as well (Zhou and Kyte, 1988), because of remaining virtually constant during surface weathering and alteration of rocks (Hayashi et al., 1997). Volcanic activity not only generated volcanic-sedimentary Mn ore deposit (Liakopoulos et al., 2001; Nyame et al., 2002), but also provided source materials for other types of Mn deposits (Fan and Yang, 1999; Levasseur et al., 2004).

An important source of the manganese in this area probably came from sea-floor volcanism or hydrothermal activity, perhaps associated with syn-sedimentary faults. This is supported by the presence of argillaceous volcanic rock in the Gufeng formation of Permian of the Lower Yangtze area (Kametaka et al., 2005; Xia et al., 1994, 1995; Yang and Yao, 2008; Zhu et al., 2012) and Early Permian magmatism in southeastern China coastal region (Li et al., 2012b). Moreover, the extremely high Mn/Fe ratios of Mn ores (>5, up to 39.7; Table 2) are consistent with fractionation of manganese and iron during hydrothermal transport and mineralization (Glasby, 2000). Geological and geochemical characteristics suggest that a magmatic heat source was available to drive hydrothermal fluids and these fluids may have played an important role in leaching and transporting metals.

Previous authors proposed that many mineral species could be formed as a result of biological activity in geological environments (Lowenstan and Weiner, 1989; Simkiss and Wilbur, 1989). Skinner (1993) discussed the distribution, size, and composition of several minerals (apatite, iron and Mn minerals), indicating that biologic effect controls on their formation. These are called bioindicator minerals, or biominerals. Some authors proposed the origin of Mn-carbonate deposits related to the decomposition of organic matter during early diagenesis (Hein and Kosk, 1987; Okita et al., 1988; Polgári et al., 1991). The carbon isotopic data of the Mn carbonate ores and Mn-bearing limestones from Permian manganese deposits of southern China ($-2.97‰ \sim -10.2‰$) show contributions of carbon from marine organic matter (Fig. 8 and Table 4). Hydrothermal activity was beneficial to the reproduction of living creature and generally increased biological activity. This is

consistent with the presence of abundant fossils in Mn-bearing limestone and shale seen within the study area.

5.2. Sedimentary environment of Guichi manganese deposits

Wright and Holser (1987) proposed that Ce anomaly ($Ce_{anom.}$) is a good index to describe the relation among Ce and La, Ce and Nd as, $Ce_{anom.} = \log\ [3 \times Ce_N/(2 \times La_N + Nd_N)]$ (shale-normalized Mclennan, 1989). The $Ce_{anom.}$ value reflects oxidation–reduction condition of ancient seawater. For example, when the $Ce_{anom.} > -0.1$, which in turn indicates that the water body was deficient in oxygen, whereas a $Ce_{anom.} < -0.1$ is taken as representing a negative anomaly Ce, and shows the sedimentary water body was oxidative (Wright and Holser, 1987). $Ce_{anom.}$ values of all samples in Guichi region are <−0.1 (Table 3), suggesting deposition took place in a well oxygenated environment. The negative Ce anomalies of the analyzed samples (Fig. 6A) probably reflect the contribution of seawater to the REE composition because seawater generally has a large negative Ce anomaly (Piepgras and Jacobsen, 1992).

The shale and chondrite-normalized cerium (Ce^*) are useful discriminants between samples and plate tectonic environments, because it is resistant to later geologic processes (Murray et al., 1990). Three depositional regimes can be identified: spreading ridge proximal with $Ce^* \sim 0.29\pm$, ocean basin floor with $Ce^* \sim 0.55$, continental margin with $Ce^* \sim 09–1.3$ (Murray et al., 1990). Therefore, the Guichi manganese district formed mostly in a marine basin (average 0.58, Table 3). This is consistent with the result indicated by the La_n/Ce_n vs. $Al_2O_3/(Al_2O_3 + Fe_2O_3)$ diagram (Fig. 7).

Sr concentrations in Mn ore covary with seawater salinity, namely Sr concentrations in seawater decrease with decreasing salinity (Klein et al., 1996). With increase of seawater temperature and salinity, Sr concentrations increase (Dueñas-Bohórquez et al., 2009). The high Sr contents of Mn-ore samples (more than 1500 ppm) indicate the Guichi manganese deposits mostly formed in high-salinity marine sedimentary environment (Dueñas-Bohórquez et al., 2009; Fan, 1994; Klein et al., 1996; Zhao, 1997).

5.3. Origin of the Guichi manganese deposits

Based on mineralogy, composition and tectonic settings, sedimentary manganese ore deposits are usually divided into three genetic types: hydrogenous, diagenetic, and hydrothermal (Bolton et al., 1988; Hein et al., 1997). Hydrogenous manganese deposits are represented by ferromanganese crusts, which slowly precipitate from seawater (2–10 mm/Myr) (Ingram et al., 1990), and are

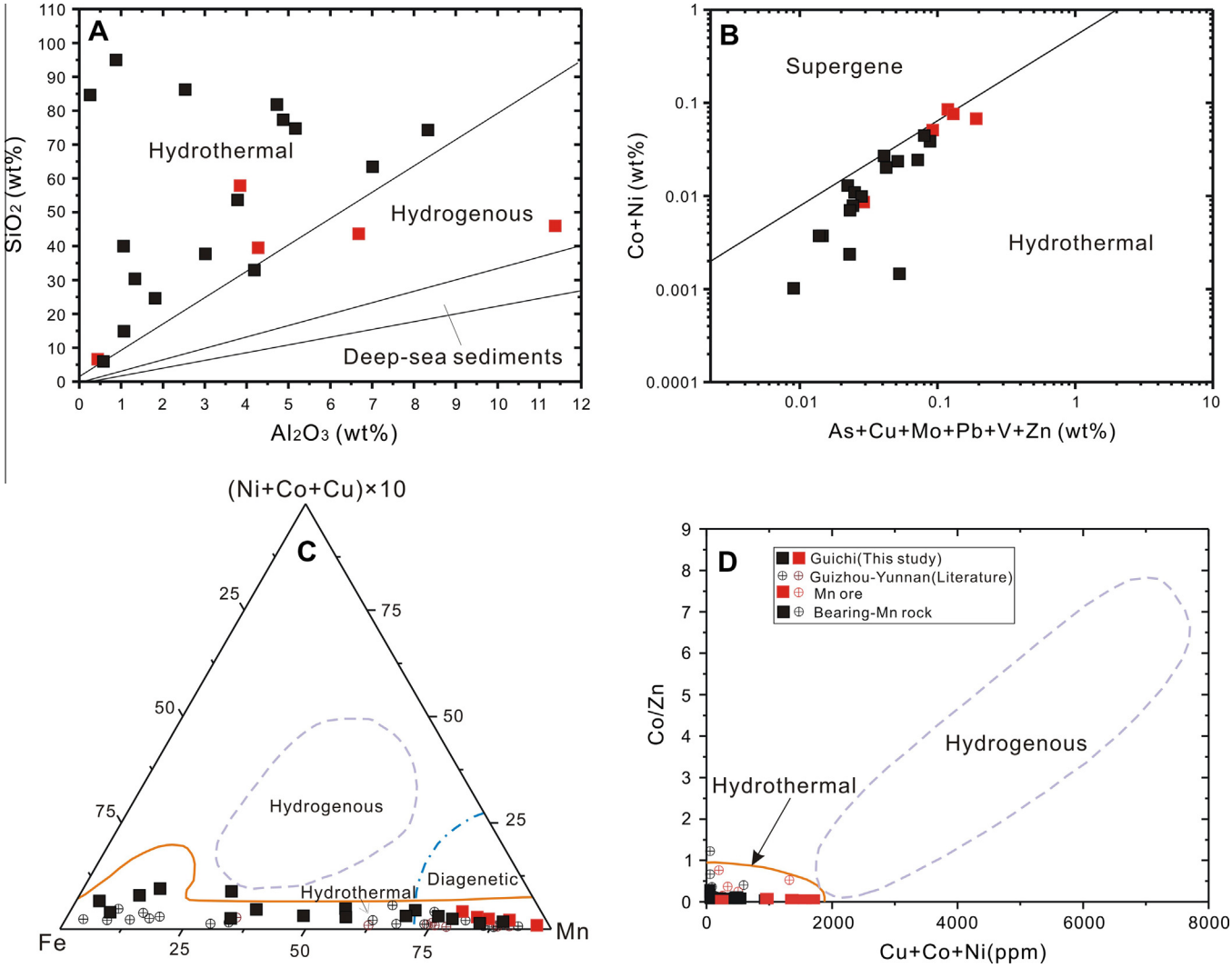

Fig. 9. Bivariate and ternary diagrams illustrating the hydrothermal components of the Permian sedimentary manganiferous formation from Guichi region in China. (A) SiO_2 –Al_2O_3 diagram (Wonder et al., 1988). (B) Diagnostic plot to discriminate between hydrothermal and supergene manganese oxides (Nicholson, 1992). (C) Fe–Mn–(Ni + Co + Cu) × 10 ternary diagram (Hein et al., 1994). (D) Co/Zn vs. Co + Ni + Cu bivariate diagram (Toth, 1980). Data for Guizhou–Yunnan are from Liu et al. (2008) and Yang et al. (2009).

characterized by a Mn/Fe ratio close to 1, high Ni and Cu concentrations (>3000 ppm), and negative Ce anomaly (Oksuz, 2011 and references therein). Diagenetic manganese deposits result from direct precipitation of Mn during early diagenesis at or below the seafloor, which is generally related to a change of redox conditions (Coleman, 1985; Hein and Kosk, 1987; Okita et al., 1988; Polgári et al., 1991). These diagenetic deposits may be composed of Mn carbonates or oxides. Hydrothermal manganese deposits which are characterized by high Mn/Fe and low trace metal concentrations (Hein et al., 1996; Hein et al., 1994), are directly precipitated from low-temperature hydrothermal solutions (Hein et al., 1997; Ingram et al., 1990) and generally have laminated and stratabound forms (Hein et al., 1997).

SiO_2 and Al_2O_3 are good indicators for the source of sediments (Wonder et al., 1988). Plotted on a SiO_2–Al_2O_3 diagram, most of the samples from the Guichi manganese district fall in the field of hydrothermal origin, with a few in the hydrogenous field (Fig. 9A). Elements such as Ba, Cu, Ni, Co, Pb, Sr, V, and Zn are frequently found in hydrothermal manganese-rich systems (Nicholson, 1992). All these elements are present in significant concentrations in the manganese ores from the Guichi region (Table 3). It has also been recognized that hydrothermal oxides are lower in Co, Cu, Ni, and Zn, relative to hydrogenous deposits. Therefore, high cobalt concentrations are indicative of marine environments as pointed out in the discrimination diagram between marine-freshwater vs. hydrothermal deposits (Nicholson, 1992). The Guichi manganese samples have low cobalt concentrations (Table 3), and plot within the hydrothermal field (Fig. 9B). Moreover, the source of metallic components of the manganiferous formation of the present study can be constrained from Mn source-discrimination diagrams (Hein et al., 1994; Toth, 1980). Consistently, the geochemical data of the manganiferous formation plot in the field of hydrothermal Mn deposits on Fe–Mn–10(Ni + Co + Cu) ternary diagrams (Hein et al., 1994) and Co/Zn vs. Co + Ni + Cu (Toth, 1980) (Fig. 9C and D).

As shown in Fig. 6A, REE patterns of the Guichi manganese deposits show a Eu anomaly, again suggesting main contribution of a hydrothermal component. The La_n/Ce_n ratios of the Mn-ores and Mn-bearing rocks (Fig. 7) also suggest main contribution of a hydrothermal component to the REE composition. In addition, high MnO/TiO_2 ratios (up to 1877 of ores) and Ba contents of Mn-ores and Mn-bearing rocks indicate that they are affected by volcanic activity and sedimentation (Oksuz, 2011).

Xia et al. (1995) once proposed that silicilite of the Permian Gufeng Formation in the Lower Yangtze area was hydrothermal sediment origin, whereas Zeng et al. (2004) proposed that cherts of Permian in Tongling region were origin of the consequence of episodic, multi-cycle activities of hydrothermal solution. Li et al. (2012b) found the ubiquitous existence of ca 280 Ma detrital zircons in the studied sediments, implying a widespread occurrence of Early Permian magmatic rocks in southeastern China coastal region. The palaeotemperatures of Mn-carbonate samples (49–71 °C) were obviously higher than those of Qixia period (35–40 °C) in the Lower Yangtze area (Jiang et al., 1994), supporting hydrothermal deposition in the Guichi region, too. Therefore, the Guichi manganese deposits are mainly of hydrothermal origin.

5.4. Genesis of siliceous rock of the Gufeng formation

The Gufeng Formation of the Middle Permian in South China is bedded siliceous rocks with tens of meters thickness. The origin of the bedded siliceous rocks is a matter of a long-term debate, with different models ranging from hydrothermal genesis (Adachi et al., 1986; Xia et al., 1995; Zeng et al., 2004), to biogenesis (Garrison and Fischer, 1969; Yang and Yao, 2008; Zhu et al., 2012), and upwelling genesis (Kametaka et al., 2005; Lü and Zhai, 1989). Silicalites of Gufeng formation from Guichi region are mainly characterized by hydrothermal sedimentary rock: high SiO_2 and Ni contents, low Al_2O_3, K_2O, P_2O_5 and Co contents, low SiO_2/Al_2O_3, $SiO_2/(K_2O + Na_2O)$, SiO_2/MgO, MnO/TiO_2 ratios, Co/Ni < 1, U/Th > 1. As discussed above, the Eu anomalies of the analyzed samples (Fig. 6A) suggest main contribution by a hydrothermal component to the Gufeng basin. In addition, the La_n/Ce_n ratios of the samples (Fig. 7) also suggest main contribution of a hydrothermal component to the REE composition in the siliceous rocks. Moreover, silica-rich precipitates have been reported in close association with massive sulfides in a modern oceanic hydrothermal vent system, in the Central Indian Ocean (Halbach et al., 2002).

Although previous authors argued that siliceous biological activities alone have difficulties to deposit large thickness siliceous rock, such as radiolarian and sponge (Xia et al., 1995 and references therein), recent researches point out that microorganisms have a more active role in silica precipitation, fixing silica and favoring its nucleation (Jones and Renaut, 1996; Konhauser et al., 2001). In many cases, silica precipitation can be attributed to a combination of both biotic and abiotic mechanisms (Guidry and Chafetz, 2003). Hydrothermal activities may supply nutrition, and are beneficial to the reproduction of siliceous organisms and other organisms, and generally increase biological activity. This is supported by the presence of volcanic ash beds in the Gufeng formation of Permian of the Lower Yangtze area (Xia et al., 1994, 1995; Kametaka et al., 2005; Yang and Yao, 2008; Zhu et al., 2012) and shale with abundant fossils among volcanic beds (Zhu et al., 2012).

On the basis of the above discussion, the Gufeng siliceous rock is very likely to be of hydrothermal origin.

6. Conclusions

(1) The Guichi manganese district of southern Anhui Province, including Tangtian, Pailou, Huikeng, Huaduling and Maya manganese deposits, occur in calcareous, argillaceous and siliceous marine sedimentary assembles of the Permian Gufeng Formation. The manganese ore bodies are layers in Mn-bearing sequence. Ore types of manganese deposits are primarily divided into primary manganese carbonate ore and manganese oxide ore, with Mn-ore grades of 18.2–45.4 wt.%.

(2) The ores are characterized by high Mn, Fe, P, Sr (more than 1500 ppm) and Ni contents (>480 ppm), Mn/Fe (>5) and La_n/Ce_n (>2) values, and low concentrations of Ca, Si and Co/Ni (<0.05) ratios, compared to Mn-bearing rocks and wallrocks. The trace element characteristics of Guichi manganese deposits have low Co/Ni (<1) and Co/Zn ratios, low in total REE contents (mostly < 100 ppm) with LREE enrichments ($(La/Yb)_N = 6.65–13.9$), negative Eu (0.46–0.75) and Ce (0.42–0.76) anomalies, and typically low $Ce_{anom.}$ (<−0.1).

(3) The $\delta^{13}C_{V\text{-}PDB}$ (−4.1‰ to 5‰) values of Mn-bearing limestone and manganese carbonate ore in the Guichi region indicate that the carbon was primary derived from Early Permian seawater with minor contributions from organic matters. The $\delta^{18}O_{V\text{-}PDB}$ (−3.4‰ to −9.9‰) values also show a similar marine source.

(4) The mineralogical and geochemical characteristics of manganese deposits in the Guichi region mainly support a hydrothermal origin and high-salinity and oxidative of marine sedimentary environment. Geochemical characteristics of the Gufeng siliceous rock likely indicate a hydrothermal origin. The multiple sources of manganese include volcanic materials, terrigenous materials and organic matter.

Acknowledgements

This study was supported by Research Fund for Doctoral Programs of Higher Education of China (No. 20100111120012), the National Natural Science Foundation of China (Grant No. 40830426), the Knowledge Innovation Project of Chinese Academy of Sciences (KZCX1-YW-15-3), and prospecting project of Anhui Bureau of Land and Resources. Prof. Yinfo Chang is highly appreciated for constructive suggestion. We also thank colleagues of Anhui Academy of Geological Survey for their help during the field study. This is contribution No. IS-0000 from GIGCAS.

References

Adachi, M., Yamamoto, K., Sugisaki, R., 1986. Hydrothermal chert and associated siliceous rocks from the northern Pacific their geological significance as indication of ocean ridge activity. Sedimentary Geology 47, 125–148.

Bau, M., Möller, P., Dulski, P., 1996. Yttrium and lanthanides in eastern Mediterranean seawater and their fractionation during redox-cycling. Marine Chemistry 56, 123–131.

Bolton, B.R., Both, R., Exon, N.F., Hamilton, T.F., Ostwald, J., Smith, J.D., 1988. Geochemistry and mineralogy of seafloor hydrothermal and hydrogenetic Mn oxide deposits from the Manus Basin and Bismarck Archipelago region of the southwest Pacific Ocean. Marine Geology 85, 65–87.

Brusnitsyn, A.I., Zhukov, I.G., 2012. Manganese deposits of the Devonian Magnitogorsk palaeovolcanic belt (Southern Urals, Russia). Ore Geology Reviews. http://dx.doi.org/10.1016/j.oregeorev.2012.01.003.

Chang, Y.F., Liu, X.P., Wu, Y.C., 1991. The Copper–Iron Belt of the Middle and Lower Reaches of the Changjiang River. Geological Publishing House, Beijing, 379 pp.

Coleman, M.L., 1985. Geochemistry of diagenetic non-silicate minerals: kinetic considerations. Philosophical Transactions of the Royal Society of London A315, 39–56.

Dubinin, A.V., Volkov, I.I., 1986. Rare earth elements in metalliferous sediments of the East Pacific Rise. Geokhimija 5, 645–662.

Dueñas-Bohórquez, A., Elisabeth da Rocha, R., Kuroyanagi, A., Bijma, B., Reichart, G.J., 2009. Effect of salinity and seawater calcite saturation state on Mg and Sr incorporation in cultured planktonic foraminifera. Marine Micropaleontology 73, 178–189.

Fürsich, F.T., Singh, I.B., Joachimski, M., Krumm, S., Schlirf, M., Schlirf, S., 2005. Palaeoclimate reconstructions of the Middle Jurassic of Kachchh (western India): an integrated approach based on palaeoecological, oxygen isotopic, and clay mineralogical data. Palaeogeography, Palaeoclimatology, Palaeoecology 217, 289–309.

Fan, D.L., 1994. Geological and Geochemical Research of the Manganese Ore Bed. Weather Publishing Press, Beijing.

Fan, D.L., Yang, P., 1999. Introduce to and classification of manganese deposits of China. Ore Geology Reviews 15, 1–15.

Fan, D.L., Ye, J., Li, J.J., 1999. Geology, mineralogy, and geochemistry of the Middle Proterozoic Wafangzi ferromanganese deposit, Liaoning Province, China. Ore Geology Reviews 15, 31–53.

Fitzgerald, C.E., Gillis, K.M., 2006. Hydrothermal manganese oxide deposits from Baby Bare seamount in the Northeast Pacific Ocean. Marine Geology 225, 145–156.

Garrison, R.E., Fischer, A.G., 1969. Deep-water limestones and radiolarites of the Alpine Jurassic. Depositional Environments in Carbonate Rocks, 20–56.

Glasby, G.P., 2000. Manganese: predominant role of nodules and crust. In: Schulz, H.D., Zabel, M. (Eds.), Marine Geochemistry. Springer-Verlag, Berlin.

Gromet, L.P., Dymek, R.F., Haskin, L.A., Korotev, R.L., 1984. The "North American Shale Composite": its compilation, major and trace element characteristics. Geochimica et Cosmochimica Acta 48, 2469–2482.

Guidry, S.A., Chafetz, H.S., 2003. Anatomy of siliceous hot springs: examples from Yellowstone National Park, Wyoming, USA. Sedimentary Geology 157, 71–106.

Halbach, M., Halbach, P., Lqders, V., 2002. Sulfide-impregnated and pure silica precipitates of hydrothermal origin from the Central Indian Ocean. Chemical Geology 182, 357–375.

Harmon, R.S., Hoefs, J., 1995. Oxygen isotope heterogeneity of the mantle deduced from global 18O systematics of basalts from different geotectonic settings. Contributions to Mineralogy and Petrology 120, 95–114.

Hayashi, K.I., Fujisawa, H., Holland, H.D., Ohmoto, H., 1997. Geochemistry of 1.9 Ga sedimentary rocks from northeastern Labrador, Canada. Geochimica et Cosmochimica Acta 61, 4115–4137.

Hein, J.R., Fan, D.L., Ye, J., Liu, T.B., Yeh, H.W., 1999. Composition and origin of Early Cambrian Tiantaishan phosphorite-Mn carbonate ores, Shaanxi Province, China. Ore Geology Reviews 15, 95–134.

Hein, J.R., Gibbs, A.E., Clague, D., Torresan, M., 1996. Hydrothermal mineralization along submarine rift zones, Hawaii. Marine Georesources Geotechnology 14, 177–203.

Hein, J.R., Koschinsky, A., Halbach, P., Manheim, F.T., Bau, M., Kang, J.-K., Lubick, N., 1997. Iron and manganese oxide mineralization in the Pacific, In: Nicholson, K., Hein, J.R., Bühn, B., Desgupta, S. (Ed.), Manganese Mineralization: Geochemistry and Mineralogy of Terrestrial and Marine Deposits. Geological Society Special Publication, pp. 123–138.

Hein, J.R., Kosk, R.A., 1987. Bacterially mediated diagenetic origin for chert-hosted manganese deposits in the Franciscan Complex, California Coast Range. Geology 15, 722–726.

Hein, J.R., Yeh, H.-W., Gunn, S.H., Gibbs, A.E., Wang, C.-H., 1994. Composition of hydrothermal ironstones from central Pacific seamounts. Geochimica et Cosmochimica Acta 58, 179–189.

Hoefs, J., 1997. Stable Isotope Geochemistry. Springer-Verlag, Berlin.

Ingram, B.L., Hein, J.R., Farmer, G.L., 1990. Age determinations and growth rates of Pacific ferromanganese deposits using strontium isotopes. Geochimica et Cosmochimica Acta 54, 1709–1721.

Irwin, H., Curtis, C., Coleman, M., 1977. Isotopic evidence for source of diagenetic carbonates formed during burial of organic-rich sediments. Nature 269, 209–213.

Jach, R., Dudek, T., 2005. Origin of a Toarcian manganese carbonate/silicate deposit from the Krížna unit, Tatra Mountains, Poland. Chemical Geology 224, 136–152.

Jiang, N.Y., Jia, R.F., Wang, Z.Y., 1994. Permain Palaeogeography and Geochemical Environment in Lower Yangtze Region. Petroleum Industry Press, Beijing, China.

Jones, B., Renaut, R.W., 1996. Influence of thermophilic bacteria on calcite and silica precipitation in hot springs with water temperatures above 90 °C: evidence from Kenya and New Zealand. Canadian Journal of Earth Sciences 33, 72–83.

Kametaka, M., Takebe, M., Nagai, H., Zhu, S.Z., Takayanagi, Y., 2005. Sedimentary environments of the Middle Permian phosphorite–chert complex from the northeastern Yangtze platform, China; the Gufeng Formation: a continental shelf radiolarian chert. Sedimentary Geology 174, 197–222.

Klein, R.T., Lohmann, K.C., Thayer, C.W., 1996. Sr/Ca and $^{13}C/^{12}C$ ratios in skeletal calcite of MytiZus trossulus: Covariation with metabolic rate, salinity, and carbon isotopic composition of seawater. Geochimica et Cosmochimica Acta 60, 4207–4221.

Konhauser, K.O., Phoenix, V.R., Bottrell, S.H., Adams, D.G., Head, I.M., 2001. Microbial–silica interactions in Icelandic hot spring sinter: possible analogues for some Precambrian siliceous stromatolites. Sedimentology 48, 415–433.

Lü, B.Q., Zhai, J.Z., 1989. Anoxic environmental sedimentation formed by Early Permian transgression and upwelling current in the areas along the lower Yangtze region. Chinese Science Bulletin 34, 1721–1724 (in Chinese with English abstract).

Lafaye, F.G., Weber, F., 2003. Natural nuclear fission reactors: time comstraints for occurrence, and their relation to uranium and manganese deposits and to the evolution of the atmosphere. Precambrian Research 20, 81–100.

Levasseur, S., Frank, M., Hein, J.R., Halliday, A.N., 2004. The global variation in the iron isotope composition of marine hydrogenetic ferromanganese deposits: implications for seawater chemistry? Earth and Planetary Science Letters 224, 91–105.

Li, H., Ling, M.X., Li, C.Y., Zhang, H., Ding, X., Yang, X.Y., Fan, W.M., Li, Y.L., Sun, W.D., 2012a. A-type granite belts of two chemical subgroups in central eastern China: Indication of ridge subduction. Lithos 150, 26–36.

Li, H., Zhang, H., Ling, M.X., Wang, F.Y., Ding, X., Zhou, J.B., Yang, X.Y., Tu, X.L., Sun, W.D., 2011. Geochemical and zircon U–Pb study of the Huangmeijian A-type granite: implications for geological evolution of the Lower Yangtze River belt. International Geology Review 53, 499–525.

Li, X.H., Li, Z.X., He, B., Li, W.X., Li, Q.L., Gao, Y.Y., Wang, X.C., 2012b. The Early Permian active continental margin and crustal growth of the Cathaysia Block: In situ U–Pb, Lu–Hf and O isotope analyses of detrital zircons. Chemical Geology 328, 195–207.

Liakopoulos, A., Glasby, G.P., Papavassiliou, C.T., Boulegue, J., 2001. Nature and origin of the Vani manganese deposit, Misos, Greece: an overview. Ore Geology Reviews 18, 181–209.

Ling, M.X., Wang, F.Y., Ding, X., Hu, Y.H., Zhou, J.B., Zartman, R.E., Yang, X.Y., Sun, W.D., 2009. Cretaceous ridge subduction along the lower Yangtze River belt, eastern China. Economic Geology 104, 303–321.

Ling, M.X., Wang, F.Y., Ding, X., Zhou, J.B., Sun, W.D., 2011. Different origins of adakites from the Dabie Mountains and the Lower Yangtze River belt in eastern China: geochemical constraints. International Geology Review 53, 727–740.

Liu, H.J., Xue, Y.Z., 1999. Sedimentology of Triassic Dounan-type manganese deposits, western margin, Yangtze Platform, China. Ore Geology Reviews 15, 165–176.

Liu, P., Liao, Y.C., Yin, K.H., Ye, D.S., Zhu, H., Han, Z.H., Yang, G.L., 2008. Hydrothermal sedimentary manganese deposits associated to volcanic activities-Permian manganese deposit in Guizhou. Geology in China 35 (5), 992–1006 (in Chinese with English abstract).

Liu, X.F., Wang, Q.S., Gao, X.J., 1989. Manganese Deposits of Guizhou. Guizhou People's Publishing House.

Lowenstan, H.A., Weiner, S., 1989. On Biomineralization. Oxford Univ. Press, New York.

Mattey, D., Lowry, D., Macpherson, C.G., 1994. Oxygen isotope composition of mantle peridotite. Earth and Planetary Science Letters 128, 231–241.

McLennan, S.M., 1989. Rare earth elements in sedimentary rocks: influence of provenance and sedimentary processes. In: Lipin, B.R., McKay, G.A. (Ed.), Geochemistry and Mineralogy of Rare Earth Elements. Mineralogical Society of America Reviews in Mineralogy, Washington, pp. 168–200.

Munteanu, M., Marincea, S., Kasper, H.U., Zak, K., Alexe, V., Trandafir, V., Saptefrati, G., Mihalache, A., 2004. Black chert-hosted manganese deposits from the Bistritei Mountains, Eastern Carpathians (Romania): petrography, genesis and metamorphic evolution. Ore Geology Reviews 24, 45–65.

Murray, R.W., 1994. Chemical criteria to identify the depositional environment of chert: general principles and applications. Sedimentary Geology 90, 213–232.

Murray, R.W., Buchholtz ten Brink, M.R., Jones, D.L., Gerlach, D.C., Russ, G.P., 1990. Rare earth elements as indicators of different marine depositional environments. Geology 18, 268–271.

Nicholson, K., 1992. Contrasting mineralogical–geochemical signatures of manganese oxides; guides to metallogenesis. Economic Geology 87, 1253–1264.

Nyame, F.K., 2008. Petrography and geochemistry of intraclastic manganese-carbonates from the ~2.2 Ga Nsuta deposit of Ghana: significance for manganese sedimentation in the Palaeoproterozoic of West Africa. Journal of African Earth Sciences 50, 133–147.

Nyame, F.K., Beukes, N.J., Kase, K., Yamamoto, M., 2002. Compositional variations in manganese carbonate micronodules from the Lower Proterozoic Nsuta deposit, Ghana: product of authigenic precipitation or post-formational diagenesis? Sedimentary Geology 154, 159–175.

Okita, P.M., Maynard, J.B., Spiker, E.C., Force, E.R., 1988. Isotopic evidence for organic matter oxidation by manganese reduction in the formation of stratiform manganese carbonate ore. Geochimica et Cosmochimica Acta 52, 2679–2685.

Oksuz, N., 2011. Geochemical characteristics of the Eymir (Sorgun-Yozgat) manganese deposit, Turkey. Journal of Rare Earths 29 (3), 287–296.

Pack, A., Russell, S.S., Shelley, J.M.G., Van Zuilen, M., 2007. Geo-and cosmochemistry of the twin elements yttrium and holmium. Geochimica et Cosmochimica Acta 71, 4592–4608.

Pfeifer, H.R., Oberänsli, H., Epprecht, W., 1988. Geochemical evidence for a synsedimentary hydrothermal origin of Jurassic iron–manganese deposits at Gonzen (Sargans, Helvetic Alps, Switzerland). Marine Geology 84, 257–272.

Piepgras, D.J., Jacobsen, B., 1992. The behavior of rare earth elements in seawater: precise determination of variations in the North Pacific water column. Geochimica et Cosmochimica Acta 56, 1851–1862.

Polgári, M., Hein, J.R., Vigh, T., Szabó-Drubina, M., Fórizs, I., Bíró, L., Müller, A., Tóth, A.L., 2012. Microbial processes and the origin of the Úrkút manganese deposit, Hungary. Ore Geology Reviews. http://dx.doi.org/10.1016/j.oregeorev.2011.10.001.

Polgári, M., Okita, P.M., Hein, J.R., 1991. Stable isotope evidence for the origin of the Ú rkút manganese ore deposit, Hungary. Journal of Sedimentary Petrology 61, 384–393.

Polgári, M., Szabó, Z., Szabó-Drubina, M., Hein, J.R., Yeh, H.W., 2005. A porous silica rock (btripoliQ) in the footwall of the Jurassic Úrkút manganese deposit, Hungary: Composition, and origin through carbonate dissolution. Sedimentary Geology 177, 87–96.

Price, G.D., Sellwood, B.W., 1997. 'Warm' palaeotemperatures from High Late Jurassic palaeolatitudes (Falkland Plateau): ecological, environmental or diagenetic controls? Palaeogeography, Palaeoclimatology, Palaeoecology 129, 315–327.

Rosales, I., Quesada, S., Robles, S., 2004. Paleotemperature variations of Early Jurassic seawater recorded in geochemical trends of belemnites from the Basque–Cantabrian basin, Northern Spain. Palaeogeography, Palaeoclimatology, Palaeoecology 203, 253–275.

Roy, S., 2006. Sedimentary manganese metallogenesis in response to the evolution of the Earth system. Earth-Science Reviews 77, 273–305.

Salas, R.D.R., Ruiz, J., Ochoa-Landín, L., Noriega, O., Barra, F., Meza-Figueroa, D., Paz-Moreno, F., 2008. Geology, Geochemistry and Re–Os systematics of manganese deposits from the Santa Rosalía Basin and adjacent areas in Baja California Sur, México. Mineralium Deposita 43, 467–482.

Sethumadhav, M.S., Yanni, G., Mohamed, M.A., Chinnaiah, 2010. Late Archean manganese mineralization and younger supergene manganese ores in the Anmod–Bisgod region, Western Dharwar Craton, southern India: Geological characterization, palaeoenvironmental history, and geomorphological setting. Ore Geology Reviews 38, 70–89.

Simkiss, K., Wilbur, K.M., 1989. Biomineralization: Cell Biology and Mineral Deposition. Academic Press, San Diego, A.

Skinner, H.C.W., 1993. A review of apatites, iron and manganese minerals and their roles as indicators of biological activity in black shales. Precambrian Research 61, 209–229.

Sugahara, H., Sugitani, K., Mimura, K., Yamashita, F., Yamamoto, K., 2010. A systematic rare-earth elements and yttrium study of Archean cherts at the Mount Goldsworthy greenstone belt in the Pilbara Craton: implication for the origin of microfossil-bearing black cherts. Precambrian Research 177, 73–87.

Sun, S.S., McDonough, W.F., 1989. Chemical and isotopic systematics of oceanic basalts: implication for mantle composition and processes. Geological Society Special Publication 42, 313–345.

Sun, W.D., Ling, M.X., Yang, X.Y., Fan, W.M., Ding, X., Liang, H.Y., 2010. Ridge subduction and porphyry copper gold mineralization. Science in China (D) 53, 475–484.

Tang, S.Y., Liu, T.B., 1999. Origin of the early Sinian Minle manganese deposit, Hunan Province, China. Ore Geology Reviews 15, 71–78.

Taylor, S.R., Mclennan, S.M., 1985. The Continental Crust: Its Composition and Evolution. Blackwell, Oxford, UK.

Toth, J.R., 1980. Deposition of submarine crusts rich in manganese and iron. Geological Society of America Bulletin 91, 44–54.

Wierzbowski, H., 2002. Detailed oxygen and carbon isotope stratigraphy of the Oxfordian in Central Poland. International Journal of Earth Sciences 91, 303–314.

Wierzbowski, H., 2004. Carbon and oxygen isotope composition of Oxfordian-Early Kimmeridgian belemnite rostra: palaeoenvironmental implications for Late Jurassic seas. Palaeogeography, Palaeoclimatology, Palaeoecology 203, 153–168.

Wonder, J.D., Spry, P.G., Windom, K.E., 1988. Geochemistry and origin of manganese-rich rocks related to iron-formation and sulfide deposits, western Georgia. Economic Geology 83, 1070–1081.

Wright, J., Holser, W.T., 1987. Paletedox variations in ancient oceans recorded by rare earth elements in fossil apatite. Geochimica et Cosmochimica Acta 51, 631–644.

Xia, B.D., Zhong, L.R., Fang, Z., Lu, H.B., 1994. Argillaceous volcanic rock was found in Gufeng formation of Permian of the Lower Yangtze area. Geological Review 40 (1), 64–73 (in Chinese with English abstract).

Xia, B.D., Zhong, L.R., Fang, Z., Lu, H.B., 1995. The origin of cherts of the early Permian Gufeng formation in the Lower Yangtze area, eastern China. Acta Geologica Sinica 69, 125–137 (in Chinese with English abstract).

Xie, J.C., Du, J.G., Xu, W., Yang, X.Y., 2006. The geological and geochemical characteristics of manganese-bearing sequences of Guichi, Anhui Province, East China. Geological review 52, 396–408 (in Chinese with English abstract).

Xu, Y.G., Chung, S.L., Shao, H., He, B., 2010. Silicic magmas from the Emeishan large igneous province, Southwest China: petrogenesis and their link with the end-Guadalupian biological crisis. Lithos 119, 47–60.

Yang, R.D., Cheng, M.L., Wei, H.R., 2009. Geochemical characteristics and origin of a manganese deposit in the middle Permian Maokou formation in Shuicheng, Gui zhou, China. Geotectonica et Metallogenia 32, 613–619 (in Chinese with English abstract).

Yang, S.Y., Yao, J., 2008. Geochemistry and origin of siliceous rocks from the Gufeng Formation of Middle Permian in the Pingdingshan Area, Chaohu Region, Anhui Province. Geological Journal of China Universities 14, 39–48 (in Chinese with English abstract).

Yeh, H.W., 1997. Stable isotope study of insular phosphorite deposits: preliminary C- and O-isotope results on the deposit of the Lau Group, Fiji. Journal of Geological Society China 40, 401–414.

Yeh, H.W., Hein, J.R., Jie, Y., Fan, D.L., 1999. Stable isotope, chemical, and mineral compositions of the Middle Proterozoic Lijiaying Mn deposit, Shaanxi Province, China. Ore Geology Reviews 15, 55–69.

Zeng, P.S., Yang, Z.S., Meng, Y.F., Pei, F.R., Hou, Z.Q., Xu, W.Y., Wang, X.C., Tian, S.H., 2004. Petrogenesis and significance of cherts in Tongling mineralization cluster area. Anhui. Geological Review 50, 153–161 (in Chinese with English abstract).

Zeng, Y.Y., Liu, T.B., 1999. Characteristics of the Devonian Xialei manganese deposit, Guangxi Zhuang Autonomous Region, China. Ore Geology Reviews 15, 153–163.

Zhao, Z.H., 1997. Geochemistry Principle of Trace Elements. Science publishing, Beijing.

Zheng, Y.F., Chen, J.F., 2000. Geochemistry of Stable Isotope. Science publishing, Beijing.

Zhou, L., Kyte, F.T., 1988. The Permian–Triassic boundary event: a geochemical study of three Chinese sections. Earth and Planetary Science Letters 90, 411–421.

Zhu, Z.Y., Jiang, S.Y., Liu, G.X., Zhao, K.D., 2012. Precise dating of the Middle Permian: Zircon U–Pb geochronology from volcanic ash beds in the basal Gufeng Formation, Yangtze region, South China. Gondwana Research. <http://dx.doi.org/10.1016/j.gr.2012.1008.1008>.